JOURNAL OF MATERIALS SCIENCE 29 (1994) 6581–6586

Superplastic behaviour of a ceramic-based kappa/alpha Fe–10Al–1.9C material

C. K. TEO
Ordnance Development and Engineering, 15 Chin Bee Drive, Singapore 2261

O. A. RUANO
Centro Nacional de Investigaciones Metalúrgicas, CSIC, Av. de Gregorio del Amo 8, 28040 Madrid, Spain

J. WADSWORTH
Lawrence Livermore National Laboratory, Chemistry and Materials Science, P.O. Box 808, L-353, Livermore, CA 94550, USA

O. D. SHERBY
Department of Materials Science and Engineering, Stanford University, Stanford, CA 94305, USA

A fine microstructure has been developed in a Fe–10Al–1.9C material made from rapidly solidified powders. The compacted material had a microstructure containing about 50 vol% kappa phase (Fe_3AlC_x) and 50 vol% alpha phase. The creep behaviour of the material was investigated using tension and compression change in strain rate tests and elongation to failure tests. Stress exponents of 2–3 were obtained over a wide range of strain rates, and an average activation energy for creep of 245 kJ mol^{-1} was determined. A maximum elongation to failure of 1120% was obtained at 900 °C. The tensile ductility as a function of strain rate was found to follow the same behaviour of other ceramic materials wherein the elongation to failure decreases sharply with an increase in strain rate.

1. Introduction

Previous work in ultrahigh carbon steels (UHCS) [1] has shown that a very fine microstructure is required to obtain superplasticity. This fine microstructure has usually been developed through various thermomechanical processing methods applied to ingot starting materials. Another successful approach, however, has been to obtain fine-grained materials through a powder metallurgy route [2].

The present investigation centres on an evaluation of the elevated temperature superplastic properties of a fine-grained UHCS containing 10%Al and 1.9%C that was processed by hot-extrusion compaction of rapidly solidified powders.

Aluminium is added to ultrahigh carbon steels to stabilize the ferrite phase, thereby shifting the austenite transformation temperature to higher temperatures. This is beneficial because the range of superplastic forming temperature can therefore be extended. An aluminium content of 10% was selected because the activity of carbon in iron at this level is very low [3], and therefore, decarburization will not occur. The high carbon level (1.9%) was selected in order to obtain a large amount of second phase, in this case kappa (Fe_3AlC_x).

Ternary phase diagrams for the Fe–Al–C system [3] show that the Fe–10Al–1.9C alloy contains gamma-plus-kappa phases in equilibrium at temperatures above 1100 °C and alpha-plus-kappa phases in equilibrium at temperatures below 1000 °C. Caution, however, must be exercised when using these diagrams because they only represent pseudo-equilibrium conditions. From room-temperature hardness measurements on this alloy, after quenching from various temperatures, it was determined that a three-phase mixture consisting of gamma-plus-alpha-plus-kappa was present between 1000 and 1100 °C. Therefore, it was decided to evaluate the potential superplastic properties of this material at temperatures below 1000 °C where only alpha-plus-kappa exists.

2. Experimental procedure

The chemical composition of the UHCS powders selected for study is (wt %) 1.9C, 1.8Cr, 10Al, balance Fe. The powders were produced by argon-gas atomization using a rapid solidification technique. In order to obtain fully dense material, the powders were compacted by hot extrusion at 1100 °C in an evacuated mild steel can at an extrusion ratio of 16:1. A scanning electron micrograph of the as-extruded material is shown in Fig. 1. The microstructure consists of coarse and fine kappa (Fe_3AlC_x where $x = 0.5–1$) particles in an alpha (Fe–Al solid solution) matrix. The coarse particles are the undissolved kappa phase at the temperature of extrusion and the fine particles are the kappa phase that has precipitated during cooling.

0022–2461

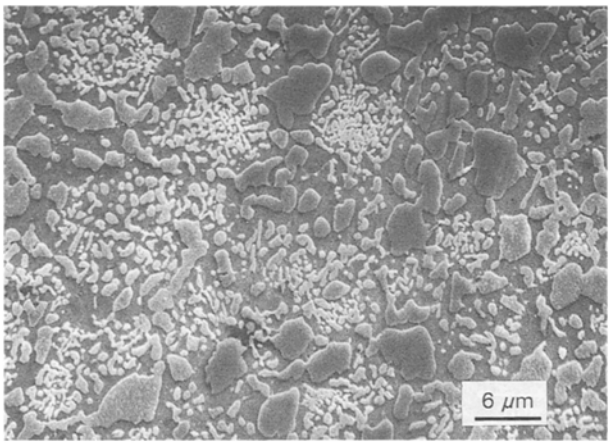

Figure 1 Scanning electron micrograph of as-extruded material showing coarse and fine kappa phase in an Fe–Al solid-solution matrix.

Transverse slices were cut from the extruded bar. Tensile samples of 6.4 mm gauge length were machined from the slices so that the tensile direction was perpendicular to the extrusion direction. As can be seen, the volume fraction of kappa phase is about 50%. Compression samples of dimensions 3.8 mm $\times$ 3.8 mm $\times$ 6.4 mm were machined from the extrusion so that the compression direction was perpendicular to the extrusion direction. Tests were carried out over the temperature range 800–900 °C, in air. In this temperature range, the two stable phases are kappa and alpha. Strain-rate change tests were used, between 1×10^{-5} and $5 \times 10^{-2}\ s^{-1}$, to determine the flow stress–strain rate relations, as well as the stress exponent, n. Initially, the samples were deformed to a level of about 20% at which point a stabilized microstructure, represented by a constant flow stress region in the stress–strain relationship, was obtained. Strain-rate change tests were performed both in tension and in compression. Direct evaluations of superplastic behaviour were performed using tensile elongation to failure tests at constant crosshead speeds. These latter tests were performed in air because virtually no oxidation occurred during testing. The samples were etched with 2% nital for optical microstructure observations. Linear intercept grain sizes, $\bar{L}$, were determined from appropriate micrographs and converted to true grain size, d, by the relation $d = 1.776\bar{L}$ [4].

3. Results and discussion

A plot of logarithm of strain rate versus logarithm of stress is shown in Fig. 2 for strain-rate change tests carried out at various temperatures. Data are shown for both tension and compression tests at 800, 850, and 900 °C. The slope of each curve yields the value of the stress exponent, n. The inverted sigmoidal shape of the curves is typical of most superplastic materials [5, 6] and defines three characteristic regions (I, II, and III). Region II is the range in which the stress exponent is at a minimum, and is often equal to about 2. In this range, it is noted that the creep rates in tension are higher than those in compression.

A plot of the strain-rate sensitivity exponent, m (defined as $1/n$), as a function of the logarithm of the

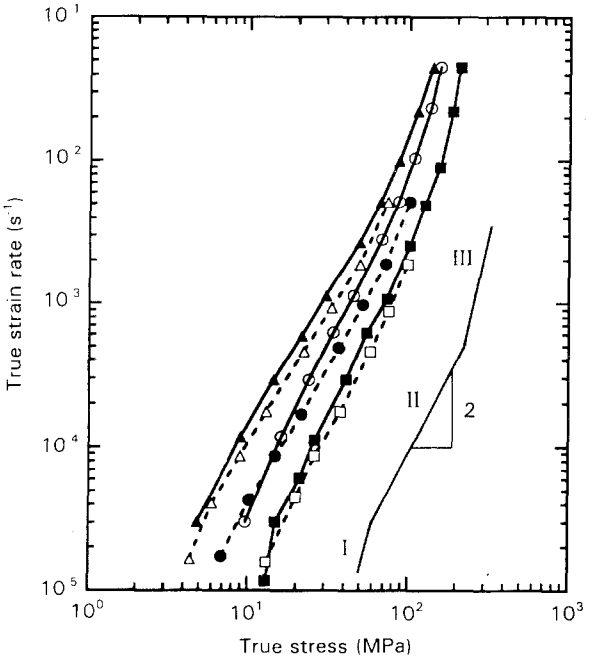

Figure 2 Comparison of strain rate versus stress data in (■, ●, ▲) tension (T) and (□, ○, △) compression (C) for Fe–10Al–1.9C at three temperatures: (□, ■) 800 °C, (○, ●) 850 °C, (△, ▲) 900 °C

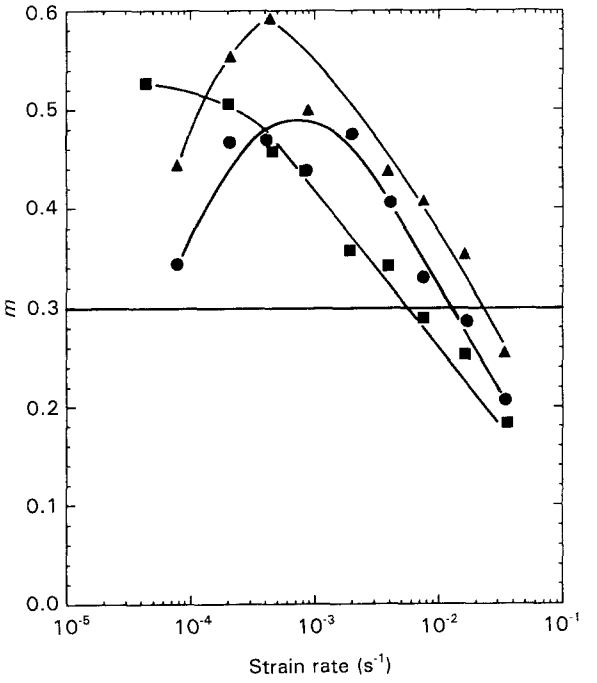

Figure 3 Strain-rate sensitivity exponent, m, as a function of strain rate for Fe–10Al–1.9C in tension, at (■) 800 °C, (●) 850 °C, (▲) 900 °C.

strain rate is shown in Fig. 3. The figure shows that the value of m goes through a maximum at each temperature. Region II, in which m is greater than 0.3, delineates the strain-rate range in which optimal superplasticity can be expected to occur. In this range, grain-boundary sliding (GBS) is believed to be the dominant deformation mechanism [6]. Region III, the high strain-rate region, where m is less than 0.3, is related to slip creep deformation mechanisms.

Microstructural changes were observed to occur during initial prestraining in the strain-rate change

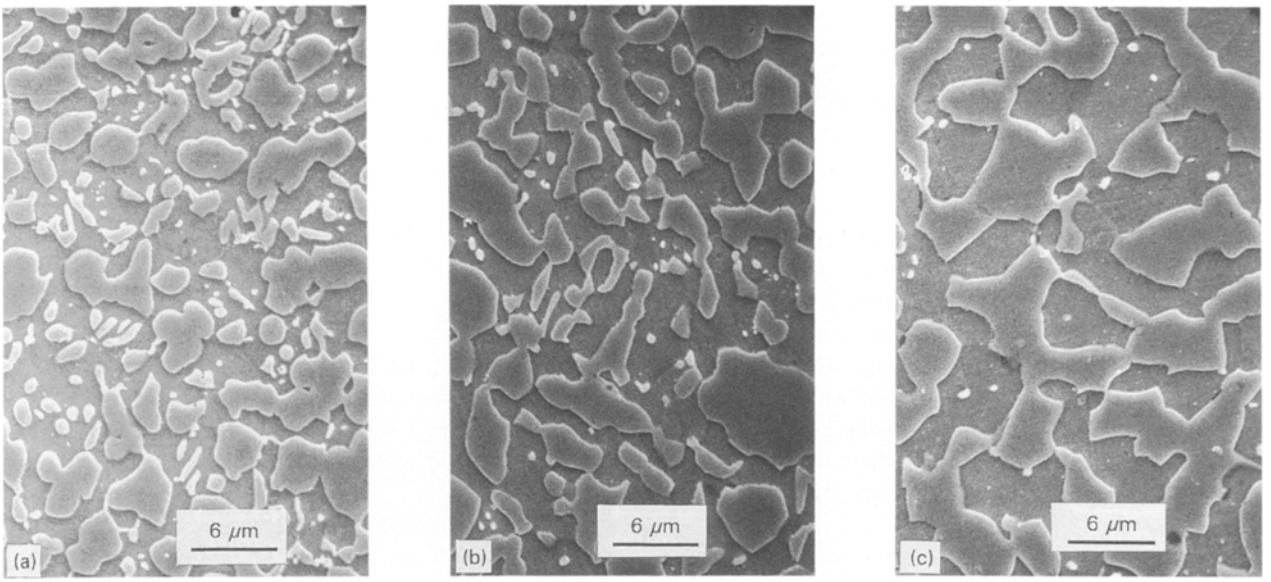

Figure 4 Scanning electron micrographs of Fe–10Al–1.9C after change in strain rate compression testing at (a) 800 °C, (b) 850 °C, and (c) 900 °C.

tests. After this prestraining region, however, only minor changes in microstructure were observed upon additional straining in the strain rate change portion of the test. The microstructural changes during prestraining were dictated by the temperature of testing. Typical microstructures, for the case of compression tests, are shown in Fig. 4. These micrographs reveal that as the testing temperature is increased, the kappa-phase distribution changes from a discontinuous type to a more continuous one. In addition, there is a grain-size increase with an increase in temperature. Similar observations were noted for the structural changes occurring during prestraining in the tensile strain-rate change tests. Grain growth was observed to be more rapid in tension than in compression. The grain size after the strain-rate change tests, in compression and tension, are documented in Table I.

A phenomenological constitutive equation that describes the behaviour of many fine-grained materials is [6]

$$\dot{\varepsilon} = A\left(\frac{\boldsymbol{b}}{d}\right)^2 (D_L/\boldsymbol{b}^2)(\sigma/E)^2 \quad (1)$$

where $\dot{\varepsilon}$ is the strain-rate, σ is the stress, A is a material constant, d is the true grain size, $\boldsymbol{b}$ is the Burgers vector, D_L is the lattice diffusion coefficient, and E is Young's modulus. The average value of A for most fine-grained materials deforming by GBS controlled by D_L is 6.4×10^9 [6]. A prediction of the value of A for Fe–10Al–1.9C was made using values for iron lattice diffusion in Fe–10Al [7], modulus data from Koster [8] for alpha iron, the grain sizes listed in Table I, and the strain rate–stress data given in Fig. 2. The average value of A was established to be 4×10^8 and is therefore about a factor of 15 less than the typical value observed in other superplastic materials. This result indicates that grain-boundary sliding in Fe–10Al–1.9C is not controlled by lattice-self-diffusion in the alpha phase. It is quite possible that grain-boundary sliding of alpha–kappa and kappa–kappa boundaries are contributing to the deformation process. Clearly, additional data regarding lattice diffusion and elastic modulus in kappa are required in order to make additional analyses. Such data are not currently available.

TABLE I True grain size of Fe–10Al–1.9C after strain-rate change tests in compression and tension

T (°C)	d (μm)	
	Compression	Tension
800	6.0	8.2
850	6.2	9.9
900	8.5	10.7

An activation energy for creep can be calculated from the data shown in Fig. 2. However, because grain growth takes place during deformation in this material, the influence of grain size on strength has to be considered in the calculation of the activation energy. Activation energy values were therefore obtained by plotting $\dot{\varepsilon}d^2$, on a logarithmic scale, as a function of reciprocal absolute temperature at a constant modulus-compensated stress (Equation 1). A value of $Q_c = 210\ \text{kJ mol}^{-1}$ was determined from the compression data, and a value of $Q_c = 245\ \text{kJ mol}^{-1}$ was determined from the tension data. The activation energy for lattice diffusion, Q_L, of iron in Fe–10Al is $270\ \text{kJ mol}^{-1}$ [7]. The comparison of Q_c with Q_L should be considered with some caution, because the values for the activation energy for creep are determined for a structure which is changing from a discontinuous to a continuous phase of kappa (the highest temperature structure is shown in Fig. 4c, and the lowest temperature structure is shown in Fig. 4a).

The data in Fig. 2 reveal that, at a given temperature, the creep rate in tension is higher than that in compression in the high strain-rate sensitivity range of stresses. Because grain growth occurred more rapidly

in the tension tests than in the compression tests, it is necessary to compare creep rates in tension and compression by normalizing for grain-size differences. This is done in Fig. 5 by plotting the grain-size compensated strain rate, $\dot{\varepsilon}d^2$, as a function of stress for the three temperatures of testing. It can be seen that after grain-size compensation, the creep rate in tension is a factor of 3–7 higher than in compression. It is believed that this difference is due to the greater ease of grain-boundary sliding when a normal tensile stress exists at the sliding boundary (as in the tension test) than when a normal compression stress exists at the boundary (as in the compression test). A similar difference has been observed in iron carbide, in the grain-boundary sliding range of stresses [9], where the creep rate in tension was about four times higher than in compression.

Constant crosshead speed tests to fracture were performed on UHCS-10Al–1.9C samples to establish the influence of initial strain rate on the high-temperature ductility of the material. Tests were conducted at 900 °C at 6.5×10^{-4}, 1.4×10^{-3}, and 3.3×10^{-3} s^{-1}. It must be pointed out that the true strain rate decreases during the test because the gauge length increases. True stress–true strain data for constant crosshead speed tests are difficult to analyse because of the number of variables incorporated in the test. Hence, correction of results to an equivalent, constant true strain rate is desirable. Sagat and Taplin [10] have reported that stress–strain curves obtained from constant crosshead tests, and subsequently corrected to to give true stress–true strain curves at constant true strain rate, coincide almost exactly with measured true stress–true strain curves obtained from constant true strain-rate tests up to a true strain of at least 1. The correction is given through the following equation.

$$\sigma_c = \sigma_v \exp[m \ln(\dot{\varepsilon}_c/\dot{\varepsilon}_v)] \quad (2)$$

where σ_v and $\dot{\varepsilon}_v$ are the values of true stress and true strain rate, respectively, obtained from the constant crosshead speed test, $\dot{\varepsilon}_c$ is the selected constant true strain rate upon which the corrected true stress σ_c is calculated.

The true corrected stress plotted as a function of the true strain is shown in Fig. 6. The corrected stresses were based on a constant strain rate equal to the initial strain rate of the constant crosshead speed test. As can be seen in the figure, the flow stress increases with increasing strain, and at constant strain the flow stress increases with increasing strain rate. The increase in flow stress with strain is attributed to strain hardening from grain growth. It is also observed, however, that the curves at the two lowest strain rates exhibit a segment of strain softening followed by rapid hardening and then terminate by fracture of the samples. Metallographic studies of microstructural changes during straining have indicated the following sequence of changes in structure that lead to an explanation of these unusual curves.

The strain-hardening regions are attributed to grain growth where GBS is the dominant deformation mechanism. The initial hardening region, prior to

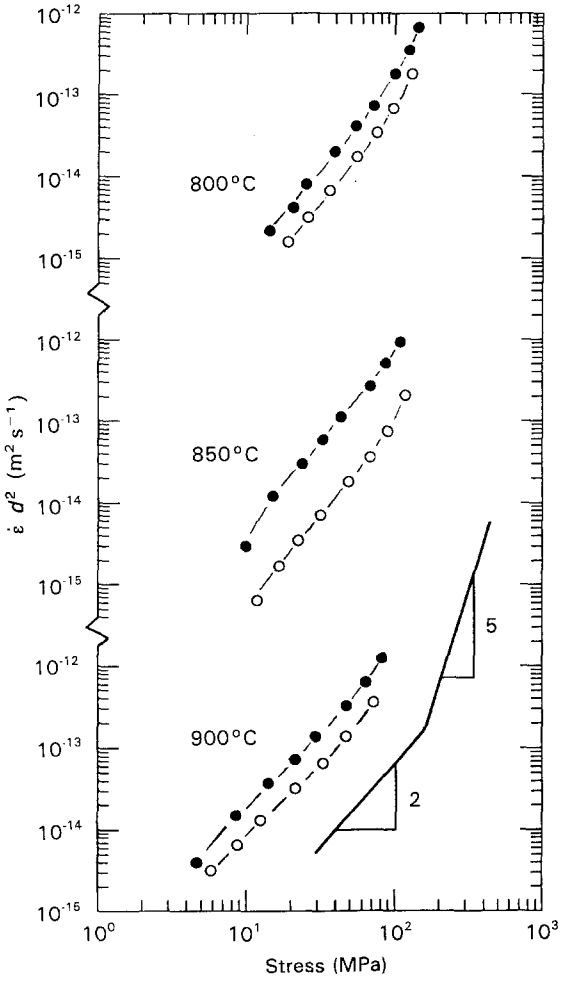

Figure 5 Comparison of grain-size compensated strain rate versus flow-stress behaviour for the Fe–10Al–1.9C material in (●) tension and (○) compression at three temperatures.

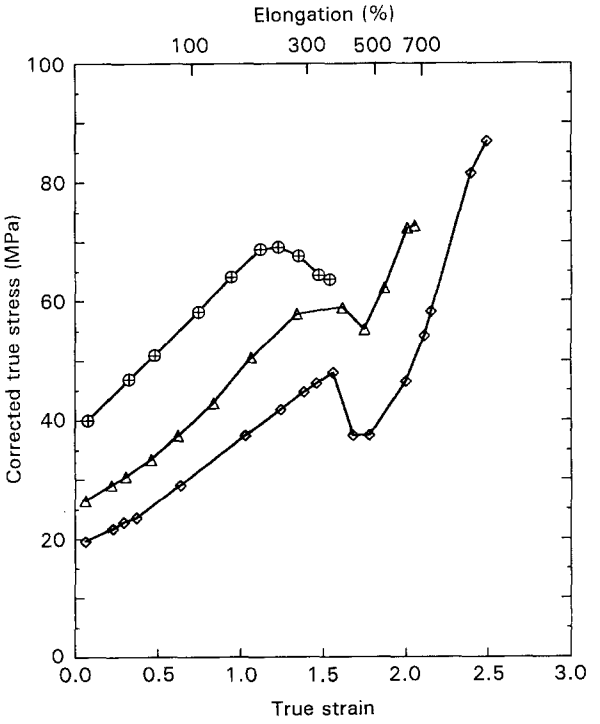

Figure 6 Corrected true stress–true strain curves for Fe–10Al–1.9C at 900 °C at three true strain rates: (◇) 6.5×10^{-4} s^{-1}, (△) 1.4×10^{-3} s^{-1}, (⊕) 3.3×10^{-3} s^{-1}. The corrected stresses were computed based on the initial strain rate of each test.

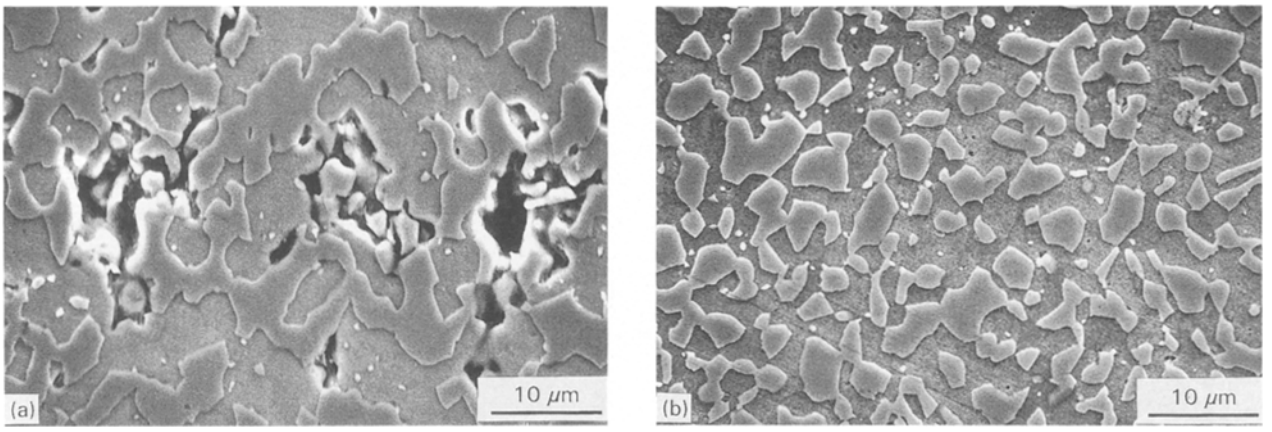

Figure 7 Scanning electron micrographs of Fe–10Al–1.9C material after elongation to failure test at 900 °C and at a constant initial strain rate of $3.3 \times 10^{-3}\ s^{-1}$; (a) gauge length region, and (b) grip region. The tensile direction is vertical.

strain softening, is related to the two-phase material with GBS in the ferrite phase playing a major role (for example, a structural state such as that shown in Fig. 4a). This is then followed by plastic instability due to local necking. But, prior to failure, sufficient straining occurs in the local region to allow the kappa phase to grow and interlink thereby preventing further deformation in the neck region. The second strain-hardening region, subsequent to strain softening, is related to the two-phase material with GBS in the continuous kappa phase playing a major role (for example, a structural state such as that shown in Fig. 4c). Eventually, when sufficient cavities and cracks have formed, failure occurs in a tensile-directed brittle-like manner.

Elongations to failure of 1120%, 700%, and 360% were achieved at constant initial strain rates of 6.5×10^{-4}, 1.4×10^{-3}, and $3.3 \times 10^{-3}\ s^{-1}$, respectively. None of the three samples showed obvious signs of local necking as noted by the sharp transverse fractures.

The microstructures of samples after the elongation to failure tests show grain growth and cavitation effects. This can be seen in Fig. 7 for the sample deformed at $3.3 \times 10^{-3}\ s^{-1}$ which shows the microstructures in the gauge length and in the grip regions. The cavities observed are large irregular voids which cannot be explained by a cavitation growth mechanism [11] because the predicted cavity sizes would be significantly smaller than those observed experimentally. The cavities shown in Fig. 7 provide proof of cavity coalescence in the deformed material. Elongated cavities were found to lie parallel to the axis of tensile straining. These types of cavities are formed by coalescence of cavities nucleated on inclusions.

As mentioned previously, the Fe–10Al–1.9C material contains kappa and alpha phases which are continuous at large strains (Fig. 7a). Because the volume fraction of kappa (a ceramic) is about equal to the volume fraction of alpha (a metal), it is not unexpected to find both ceramic- and metallic-like properties in this material. One very ceramic-like behaviour observed in the elongation to failure tests is that failure occurs without necking and the fracture surface is perpendicular to the applied tensile axis. Although fracture is brittle-like, the elongated cavities

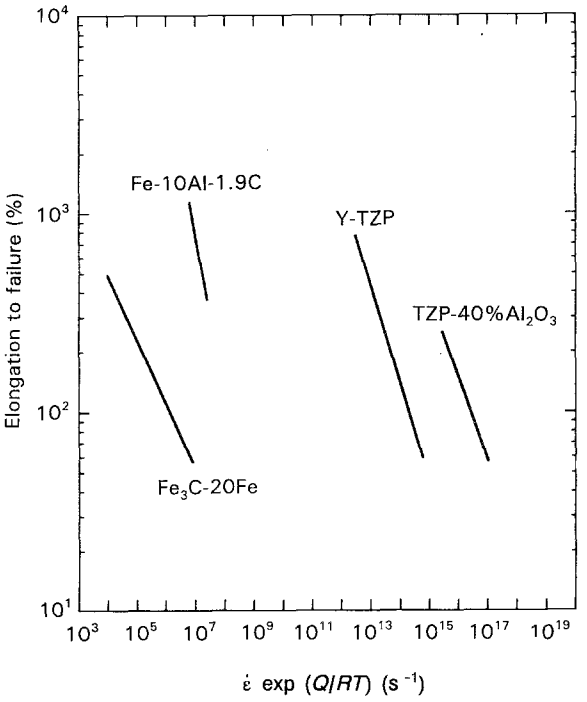

Figure 8 Tensile ductility of Fe–10Al–1.9C compared with other ceramic materials, as a function of $\dot{\varepsilon}\exp(Q/RT)$. The Q value for the Fe–10Al–1.9C material is 245 kJ mol^{-1}; Q values for the other materials are from [13].

align parallel to the applied stress, suggesting metallic-like behaviour as observed in superplastic metal-base materials [12].

Another ceramic-like characteristic can be revealed by evaluating the relationship of tensile ductility with changes in $\dot{\varepsilon}\exp(Q/RT)$. Kim *et al.* [13] have compared the tensile ductility of superplastic metallic alloys with superplastic ceramic alloys as a function of $\dot{\varepsilon}\exp(Q/RT)$. It was shown that superplastic metallic alloys show only a slight variation in tensile ductility with $\dot{\varepsilon}\exp(Q/RT)$ in the high strain-rate sensitivity range. In contrast, fine-grained ceramic materials exhibit a dramatic drop in tensile ductility with an increase in $\dot{\varepsilon}\exp(Q/RT)$, as shown in Fig. 8, even though m remains high. The figure shows that Fe–10Al–1.9C has a ceramic-like behaviour and follows the general behaviour of other ceramic materials, wherein the elongation to failure is seen to decrease sharply with an increase in strain rate.

4. Conclusions

1. Fine-grained Fe–10Al–1.9C exhibits a sigmoidal relationship between stress and strain rate, thereby defining three deformation regions.

2. At high strain rates in region III, the strain-rate sensitivity exponent, m, is less than 0.3, and creep is controlled by a dislocation slip mechanism. At intermediate strain rates in the superplastic region II, m is about 0.5 and creep is controlled by grain-boundary sliding involving diffusion in the kappa phase. An activation energy for the deformation process in this region is 245 kJ mol^{-1}.

3. The creep rate of the Fe–10Al–1.9C material is higher in tension than in compression in the high strain-rate sensitivity range.

4. Fe–10Al–1.9C exhibits excellent superplastic properties at high temperature. An elongation to failure of 1120% was obtained at 900 °C.

5. The Fe–10Al–1.9C material, which contains continuous kappa and alpha phases at large strains, exhibits both ceramic- and metallic-like properties. The tensile ductility is found to follow the same behaviour as other ceramic materials wherein the elongation to failure is seen to decrease sharply with an increase in strain rate. However, the elongated cavities observed after deformation were aligned parallel to the applied stress, suggesting metallic-like behaviour.

Acknowledgements

The authors acknowledge the contributions by Professor Frommeyer, who provided the extruded material studied in this investigation. In addition, support from the Army Research Office, DAAL-03-88-K-0056, and the NATO Research Grant (0032/88) is sincerely appreciated. Part of this work was performed under the auspices of the United States Department of Energy by Lawrence Livermore National Laboratory under Contract No. W-7405-ENG-48.

References

1. O. D. SHERBY, T. OYAMA, D. W. KUM, B. WALSER and J. WADSWORTH, *J. Metals* **37** (1985) 50.
2. O. A. RUANO, L. E. EISELSTEIN and O. D. SHERBY, *Metall. Trans.* **13A** (1982) 355.
3. K. LOHBERG and W. SCHMIDT, *Arch. Eisen.* **11** (1937) 607.
4. A. BALL and M. M. HUTCHINSON, *Metal. Sci. J.* **3** (1969) 1.
5. K. A. PADMANABHAN and G. J. DAVIES, "Superplasticity" (MREZ, Springer, Berlin, 1980).
6. O. D. SHERBY and J. WADSWORTH, "Deformation, Processing, and Structures", edited by G. Krauss (ASM, Metals Park, OH, 1984) p. 355.
7. O. OIKAWA, *Tech. Rep. Tohoku Univ.* **48** (1983) 9.
8. W. KOSTER, *Z. Metall.* **39** (1948) 1.
9. W. J. KIM, J. WOLFENSTINE, O. A. RUANO, G. FROMMEYER and O. D. SHERBY, *Metall. Trans.* **23A** (1992) 527.
10. S. SAGAT and D. M. R. TAPLIN, *Metal. Sci.* **10** (1976) 94.
11. J. PILLING and N. RIDLEY, in "Superplasticity in Aerospace", edited by H. C. Heikkenen and T. R. McNelley (The Metallurgical Society, Warrendale, PA 1988) p. 183.
12. O. D. SHERBY and J. WADSWORTH, *Progr. Mater. Sci.* **33** (1989) 169.
13. W. J. KIM, J. WOLFENSTINE and O. D. SHERBY, *Acta Metall. Mater.* **39** (1991) 199.

Received 9 February 1993
and accepted 16 May 1994